Construction and Building Materials 220 (2019) 375–385

Contents lists available at ScienceDirect

Construction and Building Materials

journal homepage: www.elsevier.com/locate/conbuildmat

Iron ore tailing-based geopolymer containing glass wool residue: A study of mechanical and microstructural properties

Keoma do Carmo e Silva Defáveri [a,*], Letícia Figueiredo dos Santos [b], José Maria Franco de Carvalho [c], Ricardo André Fiorotti Peixoto [b], Guilherme Jorge Brigolini [b]

[a] Departamento de Engenharia, Universidade Federal de Lavras (UFLA), Campus Universitário Lavras, 37200-000 Lavras, Minas Gerais, Brazil
[b] Laboratório de Materiais de Construção Civil, Escola de Minas, Universidade Federal de Ouro Preto (UFOP), Campus Universitário, Morro do Cruzeiro, 35400-000 Ouro Preto, Minas Gerais, Brazil
[c] Laboratório de Engenharia Civil, Departamento de Engenharia Civil, Universidade Federal de Viçosa (UFV), Campus Universitário, 36570-900 Viçosa, Minas Gerais, Brazil

HIGHLIGHTS

- The application of iron ore tailing as primary source material to geopolymerization.
- Effect of glass wool residue as a blend for iron ore tailing-based geopolymer.
- High mechanical performance at 7 days of curing was observed for the geopolymers.
- Glass wool residue led to a reduction in mechanical strength.

ARTICLE INFO

Article history:
Received 30 December 2018
Received in revised form 26 April 2019
Accepted 29 May 2019
Available online 11 June 2019

Keywords:
Iron ore tailing
Glass wool residue
Geopolymer
Zeolite
Microstructure
Rietveld

ABSTRACT

This work presents an evaluation of the application of iron ore tailing as primary precursor material to geopolymer production. Glass wool residue from the iron ore industry was also included as a blend material. Four mixtures of geopolymers were produced: one mixture using only iron ore tailing; three mixtures where the iron ore tailing was replaced by the glass wool residue, with a substitution ratio of 10%, 20% and 30% (in mass). Furthermore, three different grinding times and three NaOH solution concentration were applied. Compressive strength and flexural strength tests were performed in prismatic specimens at 7-days, and the microstructural analysis of the fragments was obtained by SEM analysis. QXRD analysis based on the Rietveld's refinement method and TG/DTA analysis was applied for all specimens. The results showed the synthesis of a zeolite phase in all specimens, and the SEM micrographs showed a transformation process of the glass wool residue. Finally, high mechanical performances were found to the iron ore tailing-based geopolymer, reaching values higher than 100 MPa for compressive strength and 20 MPa for flexural strength. The obtained values are related to the grain packing improvements, geopolymerization products, and the glass wool residue working as a supplementary precursor material to the geopolymerization reaction. The result points to the potential of iron ore tailing and glass wool residue to geopolymers studies and application.

1. Introduction

Geopolymers are inorganic materials produced by alkaline activation of aluminosilicate materials through the geopolymerization reaction. In a highly concentrated alkali hydroxide or silicate solution, the aluminosilicates form a very stable material with amorphous or semi-crystalline polymeric structures with interconnected Si-O-Al-O-Si bonds called geopolymer [1–3]. Typical examples of precursor materials to the geopolymer synthesis are metakaolin, fly ash and slag.

Currently, Portland cement is the most used binder and one of the main responsible for the low environmental performance of conventional concrete. Cement production accounts for 5–7% of total global CO_2 emissions [4–7]. Furthermore, concrete structures under specific environmental conditions exhibit some durability problems. This important aspect related to serviceability life of the structure is the capability to resist the mechanical actions,

* Corresponding author.
E-mail addresses: keoma.silva@ufla.br (K. do Carmo e Silva Defáveri), josemaria.carvalho@ufv.br (J.M. Franco de Carvalho), guilhermebrigolini@ufop.edu.br (G.J. Brigolini).

https://doi.org/10.1016/j.conbuildmat.2019.05.181
0950-0618/

physical actions, and chemical aggressions that it is subjected to over their expected service life [8].

Geopolymer binders arise as an alternative to Portland cement with considerable advantages. They have superior durability properties such as sulfate resistance, acid resistance [9,10], fire resistance [11], and chloride ion penetrability [12]. Geopolymer samples reach high mechanical resistance in a few hours of synthesis, and its application results on environmental and economic benefits yielded by the application of residues and by-products as precursor material [13].

Brazil generates and disposes of in tailings dams around 184 million tonnes of iron ore tailings (IOT) annually [14]. For this reason, Brazilian mineral industry is investing on environmental programs that aims to residue reduction, proper disposal, improvements in the maintenance and monitoring of tailings dams [15]. In this sense, several studies have been conducted focusing on the reuse of IOT in new materials for civil construction, including the use of IOT as a recycled aggregate [16–20], pigment for sustainable paints [21], and eco-friendly bricks [22].

The iron ore industry generates other residues in the benefaction process of iron ore. Glass wool is used as insulation material for the pipes and pellets furnaces, and after service life, the material is discarded in controlled landfills as glass wool residue (GWR). However, previous research showed that this material shows pozzolanic reactivity and a predominantly amorphous structure [23].

Reviewing the previously published findings, very few researchers have studied the application of IOT as a precursor material to geopolymer synthesis. Some works show the effects of the IOT employment as a blend material to the geopolymer production [11,24]. Therefore, this paper studies the feasibility of IOT usage as the primary precursor material to the geopolymer production. Additionally, the effects of the GWR as a supplementary precursor material into the IOT-based geopolymer is also evaluated. As a result, a geopolymer material produced using two different residues from the iron ore industry was proposed, and promising results were obtained.

2. Experimental procedure

2.1. Materials

The IOT used in this study was collected from an iron ore tailings dam geographically located in the city of Ouro Preto, Brazil. The GWR was obtained from an iron ore port industrial complex located in the Espírito Santo State, Brazil. Both materials are residues generated in two different production stages of the iron ore mining industry. The chemical compositions of IOT and GWR were determined by X-Ray Fluorescence (XRF), and the mineral phase composition by quantitative X-Ray Diffraction (QXRD) based on Rietveld's refinement method [25]. Thermogravimetric and thermal differential analysis (TG/DTA) were also used in the characterization procedure.

The IOT and GWR were firstly oven dried at 100 °C for 24 h, and a grinding method was applied to yield the reactivity. The grinding times to IOT were 1 h, 2 h, and 3 h, which related powders obtained were named here as IOT-1, IOT-2, and IOT-3, respectively. The GWR was ground for 30 min and was used the fraction passed through the #320 mesh (45 μm) sieve. A laboratory horizontal ball mill (MA500, Marconi) was used to all precursor materials using 32 stainless steel spheres (diameter of 32 mm). After grinding, the particle size distribution of the powders was determined by laser diffraction using an analyzer Bettersize 2000 with isopropyl alcohol as a dispersant.

The alkaline activator applied in this research was a simple solution of sodium hydroxide in three different concentration: 8 M, 10 M, and 12 M (mol/L). The solutions were prepared by dissolving NaOH pellets (analytical grade, purity > 98%) in distilled water.

2.2. Mix design and specimen preparation

Specimens of IOT-based geopolymer (IG) were prepared, as well as IOT-based geopolymer blended with GWR (IGG). The IG specimens were produced with all activator solution concentrations (8 M, 10 M, and 12 M), and all grinding times (IOT-1, IOT-2, and IOT-3). The terminology applied was IG XY, where IG refers to precursor material, X refers to NaOH solution concentration, and Y refers to grinding time. The IGG specimens were produced for the 10 M solution concentration and 3 h of grinding time. The terminology applied was IGG KWZ, where IGG refers to precursor material and blend, K refers to NaOH solution concentration, W refers to grinding time, and Z refers to substitution ratio (i.e., IOT substitution for GWR in mass).

The mixture procedure of the IOT specimens and NaOH solution (all grinding times and solution concentrations) are described as follows. The NaOH solution was placed in the batch of the standard cement mortar mixer (JJ-5 Type), and then the solid precursor was added in sequence. The geopolymer was mechanically mixed for 3 min at slow speed, followed by more 3 min at high speed. For the blended geopolymers, the IOT and GWR were firstly manually homogenized, and then the same mixture procedure was applied. The fresh geopolymeric pastes were cast in prism molds ($40 \times 40 \times 160$ mm), and after they were compacted in a laboratory mortar flow table (30 strikes). The samples were cured in a laboratory oven (100 °C) for seven days. The liquid to solid (L/S) ratio was set at 0.27 for all samples. Table 1 shows the mixture design of the produced geopolymers.

2.3. Testing methods

Mechanical properties and microstructural characterization analysis were performed on the geopolymers samples as follows:

i. The specimen nominal density was calculated dividing its weight by its volume prior to the flexural strength test. The average value of the three specimens was taken as the result of the specific mixture.
ii. The 7-days compressive and flexural strength was measured based on the standard method [26]. Three specimens of each mixture for flexural test and six specimens of each mixture for compressive strength were tested. A hydraulic press EMIC DL 20,000 was used with a 200 kN load cell; the load increment adopted was 0.25 MPa/s. All values presented in the current work were the average values of three tests (flexural strength), and six tests (compressive strength) with the error reported as a standard deviation from the mean.
iii. Quantitative X-Ray Diffraction (QXRD) was conducted using a Bruker D2 Phaser 2nd Generation powder X-Ray diffractometer, with CuKα (1.54184 A) radiation; tube setting to

Table 1
Geopolymers mixture design.

Mixture	IOT	GWR	Liquid/Solid**
ID	(g)	(g)	(ad.)
IGG 81 – IG 123*	1500	–	0.27
IGG 10310	1350	150	
IGG 10320	1200	300	
IGG 10330	1050	450	

* Includes all specimens belonging into the range;
** IOT and GWR were both considered solids.

be 30 kV and 10 mA; a step size of 0.021°; step time of 1 s and a 2θ range of 7°–60°. The Rietveld refinement was carried using the software X'Pert HighScore Plus with the Crystallography Open Database (COD). The samples were crushed from mechanical test fragments and passed through a #200 mesh (75 μm) sieve. Two different samples of each specimen were representatively collected and used for the QXRD analysis. All results values presented in the current work were an average of two samples, with the error reported as a deviation from the mean.

iv. The simultaneous thermal analysis (TG/DTA) was performed using a Shimadzu DTG-60H instrument. The powder samples (particle size < 75 μm) were put in a platinum crucible, and heated from 25 °C to 1000 °C at 10 °C·min^{-1} rate, in an N_2 atmosphere (μl·min^{-1}). One sample of each mixture was also collected from mechanical test fragments for the TG/DTA analysis on the same day of their rupture.

v. Scanning Electron Microscopy (SEM) with energy dispersive X-Ray Spectrometry (EDS) analysis and secondary electrons (SE) was performed using a TESCAN VEGA 3 microscope. The samples were obtained from crushed specimens of the compressive strength test (fracture method) and analyzed on the same day of their rupture.

3. Results and discussion

3.1. Materials characterization

Table 2 shows the XRF results of IOT and GWR in oxides. The IOT has high amounts of silicon and iron oxide, and low amounts of aluminum oxide. The GWR presents high amounts of silicon oxide, and low amounts of aluminum, iron, and calcium oxides. IOT has a silicon to aluminum ratio (Si/Al) of 4.59, while for GWR this ratio is 2.48. Davidovits [27] argued that a Si/Al ratio between 3.2 and 4.5 is environmentally compatible, and De Silva [28] showed that an increase in the Si/Al ratio leads to longer setting times. Furthermore, the presence of CaO in GWR could lead to calcium silicate hydrate (C—S—H) compounds and $Ca(OH)_2$ precipitation in the geopolymeric system, as well as interfere on the formation of fully crystalline zeolites [29].

The XRD patterns of IOT and GWR are presented in Fig. 1. The IOT mineralogical phases are quartz, hematite, goethite, chantalite, and chamosite, while the GWR shows only non-crystalline phases. The IOT mineralogical phases are consistent with previous work [30,31,16,21], and sharp peaks of quartz and hematite dominate it. Furthermore, the aluminum phases are found associated with chantalite and chamosite. The substitution ratios of IOT by GWR (10%, 20%, and 30%, in mass) did not significantly alter the Si/Al ratio of the geopolymers composites; on the other hand, the application of GWR works as an "amorphous correction", raising the volume of available non-crystalline structures.

Table 3 shows the particle size distribution and physical properties of IOT and GWR. For IOT, the increase in grinding time for 1 h–2 h led to a reduction of only 7% in the particle size parameter D90; however, the increase of grinding time for 1 h–3 h produced a reduction in this parameter of 33%. Looking at Blaine specific surface area, the grinding time produced a significant increase comparing the results of 1 h and 2 h, which is related to the reductions in the particles size of the finer fractions (evidenced by the values of D10 and D50). The similar values of specific sur-

Table 2
Chemical elements by XRF of IOT and GWR.

Material ID	Oxide Elements							
	SiO_2 (%)	Al_2O_3 (%)	Fe_2O_3 (%)	CaO (%)	TiO_2 (%)	SO_3 (%)	Others* (%)	LOI (%)
IOT	40.0	8.7	48.9	–	–	–	1.9	6.0
GWR	43.7	17.6	12.0	19.7	2.6	1.3	2.9	5.4

* Oxide Elements values lower than 1%.

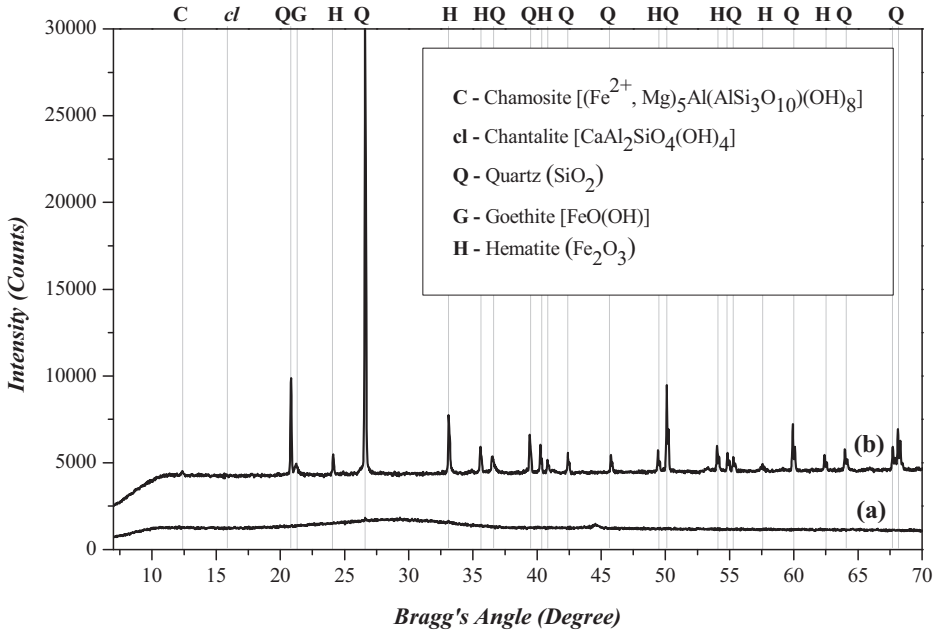

Fig. 1. XRD patterns of the evaluated materials: (a) GWR; and (b) IOT.

Table 3
Particle size distribution and physical properties of IOT and GWR.

Material ID	Particle Size Distribution			Physical Properties	
	D10 (μm)	D50 (μm)	D90 (μm)	Specific Mass (g/cm^3)	Specific Surface Area (m^2/g)
IOT-1	2.2	19.1	76.6	2.924	0.034
IOT-2	1.7	15.8	71.1	2.934	0.041
IOT-3	1.3	10.6	51.0	2.903	0.041
GWR	4.2	22.3	71.95	2.596	0.555

face area for 2 h and 3 h shows that, although the particles have become thinner, the particle shape presented an important improvement, becoming more equant and less rough. It is also noticeable the higher specific surface area of GWR in comparison to all IOT samples due to the elongated shape of its particles.

3.2. Mechanical tests

The results of nominal density are shown in Fig. 2. The IG geopolymers showed nominal density around 2–2.4 g/cm^3, highly influenced by the molar concentration of NaOH solution. The partial replacement of IOT for GWR produced slight reductions in nominal density for all substitution ratios (6–9%). The results did not differ from previous researches, which found an average density around of 2.0 g/cm^3 when using fly ash-based geopolymers [32].

Fig. 3 shows the results of the 7-days flexural strength tests. The maximum value was 21.3 MPa for IG 123, which indicates that the optimum combination was the alkali solution concentration of 12 M combined with the grinding time of 3 h. The results also show that the flexural strength tends to increase with the increase of the NaOH concentration in solution.

The partial replacement of IOT by GWR reduced the 7-days flexural strength of the geopolymers significantly (Fig. 4). All substitution ratios present an inverse proportion (i.e., when the substitution ratio increases the flexural strength decreases). The minimum strength (2.5 MPa for IGG10330) was 89.1% lower than that for IG 103. The use of fiber reinforcement in geopolymers composites commonly aims the improvement of mechanical performance, durability, and other properties. In this sense, depending on the type and amount of fibers, the literature reports an increase in the flexural strength [33,34,8]. The decrease observed in this study due to the addition of GWR may indicate that it does not work as a fiber reinforcement.

Fig. 5 shows the results of 7-days compressive strength. The maximum value observed was 112.8 MPa for IG 123 (which also showed the highest flexural strength). It can be seen that the compressive strength of IG geopolymers is increased as the NaOH solution concentration and grinding time increases.

Results also show a significant decrease in the compressive strength of the geopolymers produced with GWR compared to the correspondent IOT-based geopolymer (Fig. 6). IGG geopolymers showed a decrease in compressive strength with the increase

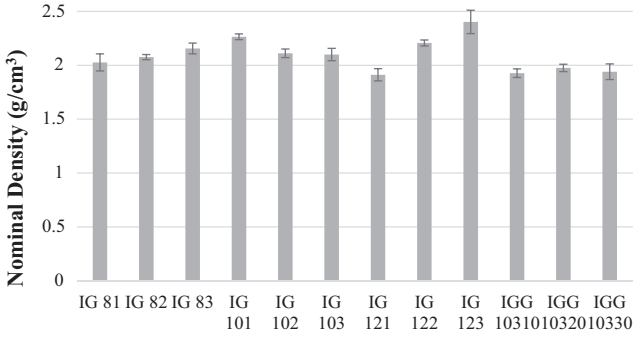

Fig. 2. Nominal density of IG and IGG specimens.

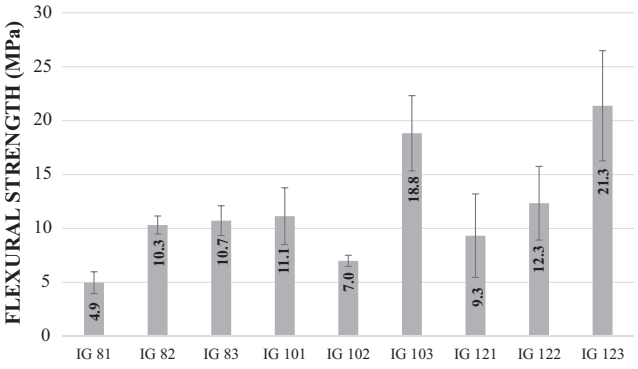

Fig. 3. Flexural strength results of IG specimens.

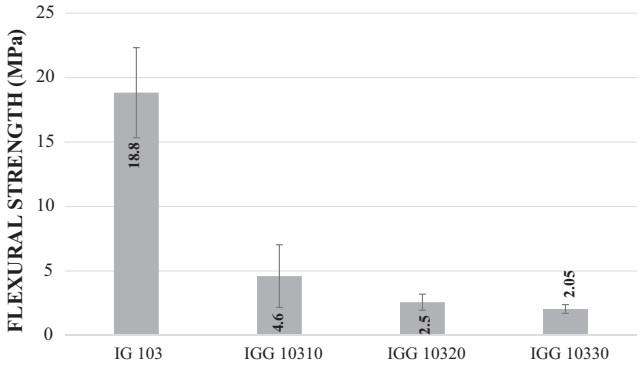

Fig. 4. Flexural strength results of IG and IGG specimens.

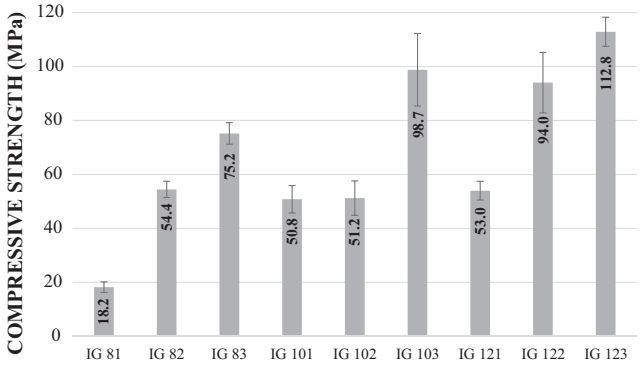

Fig. 5. Compressive strength results for IG specimens.

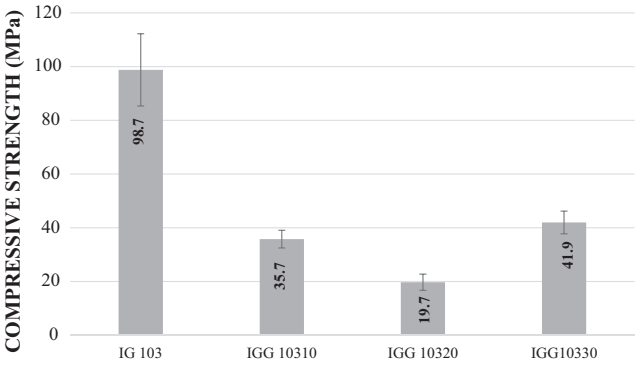

Fig. 6. Compressive strength results for IG and IGG specimens.

in the replacement ratio from 10% to 20%. On the other hand, the replacement ratio of 30% led to an improvement in mechanical performance compared to the other IGG geopolymers. Additionally, the relative reduction in standard deviations observed in the IGG geopolymers suggests a more homogeneous microstructure.

The results of compressive and flexural strength show that the fineness of the IOT and GWR play an essential role in the development of mechanical strength. Authors have agreed that the variation of the particle size distribution of the binder phase has a significant effect on the compressive strength since commonly binder phases with finer particle size distribution will yield geopolymer pastes endued with denser microstructure, refined physical properties, and higher compressive strength [35–38]. Furthermore, the parameter *D90* of GWR and the compressive strength of IGG 10330 closely related to the IOT-2 support the packing density hypothesis. On the other hand, previous research reporting the use of IOT as an addition in geopolymer found a correlation between the IOT content and C—S—H formation, a fact that lead to compressive strength improvements [11]. The mechanical performance is a parameter to evaluate the degree of geopolymerization, and in this sense, the IG and IGG geopolymers achieved compressive strength values higher than those reported for mine tailings and metakaolin based geopolymers [39,40].

3.3. Microstructural properties

The XRD patterns of the IG geopolymers are shown in Fig. 7. The significant change in the XRD patterns is the disappearance of crystalline peaks corresponding to chamosite indicating the partial dissolution and formation of the crystalline phase zeolite type (i.e., Sodalite at around 15° 2θ). This phenomenon is in close agreement with previous studies [41,42,29] and indicates a fast reorganization process after synthesis. Furthermore, the phases quartz, hematite, and goethite are possibly non-reactive and could act as inert filler, yielding the geopolymer mechanical properties by the particle arrangement.

Due to the limitations of XRD crystallinity analysis, it is common that no newly formed crystalline phases related to the geopolymeric products are identifiable [29]. The nature of aluminosilicate changes quickly on heating, and as heating progress further, the peaks become sharp peaks identifiable as zeolite-type structures [43]. Furthermore, Ríos *et al* [44] summarized the reaction from amorphous aluminosilicate gel to crystalline zeolite-types as poorly crystalline aluminosilicate → zeolite as metastable phase → sodalite. The transformation indicates a dissolution of a gel phase, nucleation and further growth of more stable phases such as sodalite, which confirms the dissolution process into the IG specimens.

Fig. 8 shows the same mineralogical behavior in the IGG geopolymers. It was observed the sodalite synthesis followed by a reduction of the chamosite and chantalite peaks. The non-crystalline phases from GWR did not produce a characteristic "hump" in the XRD pattern by visual analysis. However, was not used external or internal standard on the tested specimens, as a result, the amorphous content was not quantitatively evaluated in the present work.

Table 4 shows the results of the QXRD analysis of IG and IGG geopolymers. The decrease in sodalite content related to the increase in grinding times was a trend observed in all IG geopolymers. For all NaOH solutions, the grinding time of 3 h yielded similar contents of sodalite. IGG data also shows similar values of sodalite for all replacement ratios. Higher chantalite contents were observed in IGG geopolymers in comparison to IG ones. This fact

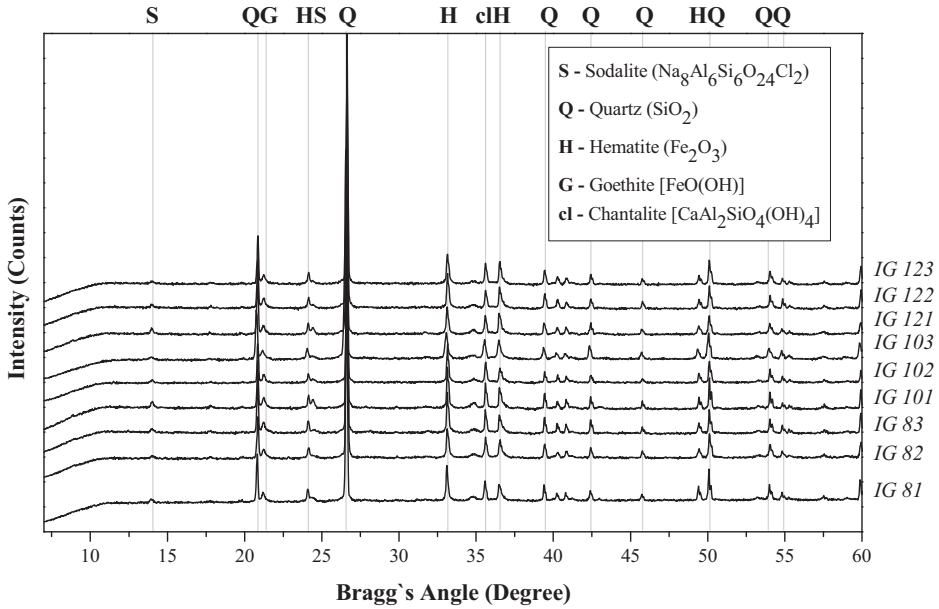

Fig. 7. QXRD patterns of IG specimens at 7 days of curing.

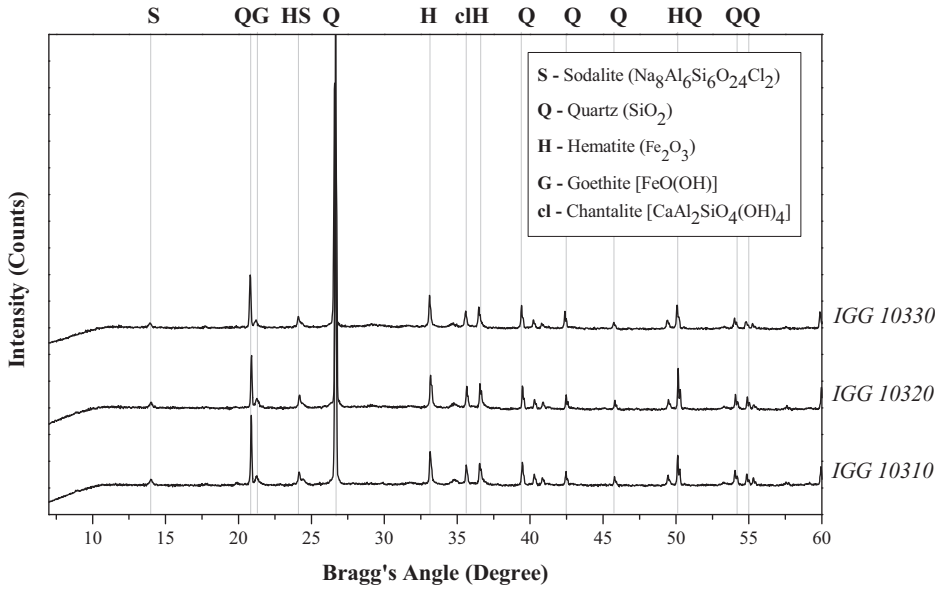

Fig. 8. QXRD patterns of IGG specimens at 7 days of curing.

Table 4
QXRD results of IG and IGG specimens at 7 days of curing.

Mixture ID	Mineral Phases*					Statistical Errors	
	Quartz (%)	Hematite (%)	Goethite (%)	Chantalite (%)	Sodalite (%)	GOF (a.d.)	RWP (a.d.)
IG 81	72.6 (±0.4)	15.5 (±0.2)	6.6 (±0.2)	0.85 (±0.2)	4.4 (±0.4)	1.88–2.14	2.36–2.55
IG 82	73.1 (±0.3)	14.5 (±0.6)	8.2 (±0.1)	1.0 (±0.1)	3.0 (±0.1)	1.85–2.11	2.31–2.51
IG 83	75.2 (±1.3)	13.4 (0.8)	7.4 (±0.0)	1.0 (±0.2)	2.9 (±0.2)	1.92–1.28	2.39–2.64
IG 101	66.5 (±1.4)	15.8 (±0.6)	8.8 (±0.7)	1.0 (±0.1)	7.8 (±0.2)	2.05–2.36	2.43–2.57
IG 102	71.3 (±1.9)	15.1 (±2.0)	8.5 (±0.1)	0.95 (±0.2)	4.0 (±0.3)	1.87–2.27	2.69–3.01
IG 103	75.9 (±1.8)	13.2 (±0.7)	6.6 (±0.7)	1.3 (±0.1)	2.85 (±0.4)	2.37–2.96	2.69–2.75
IG 121	77.8 (±1.5)	10.2 (±0.5)	5.9 (±0.7)	1.2 (±0.0)	4.9 (±0.2)	2.46–3.8	2.82–3.52
IG 122	74.4 (±1.1)	13.6 (±0.3)	7.0 (±0.7)	1.5 (±0.1)	3.3 (±0.1)	1.93–2.13	2.52–2.61
IG 123	76.4 (±3.2)	13.1 (±1.5)	6.7 (±1.6)	1.35 (±0.1)	2.4 (±0.2)	1.75–2.04	2.36–2.55
IGG 10310	72.7 (±2.3)	12.9 (±0.5)	7.3 (±1.0)	1.9 (±0.2)	5.2 (±0.6)	2.31–2.83	2.79–3.07
IGG 10320	73.7 (±0.9)	13.2 (±0.1)	7.1 (±0.4)	1.2 (±0.1)	4.7 (±0.5)	2.34–2.69	2.89–3.01
IGG 10330	74.7 (±2.1)	12.6 (±0.9)	6.1 (±1.1)	1.4 (±0.3)	5.1 (±0.5)	2.30–2.39	3.00–3.05

* Values presented followed by the deviation from the mean (%).

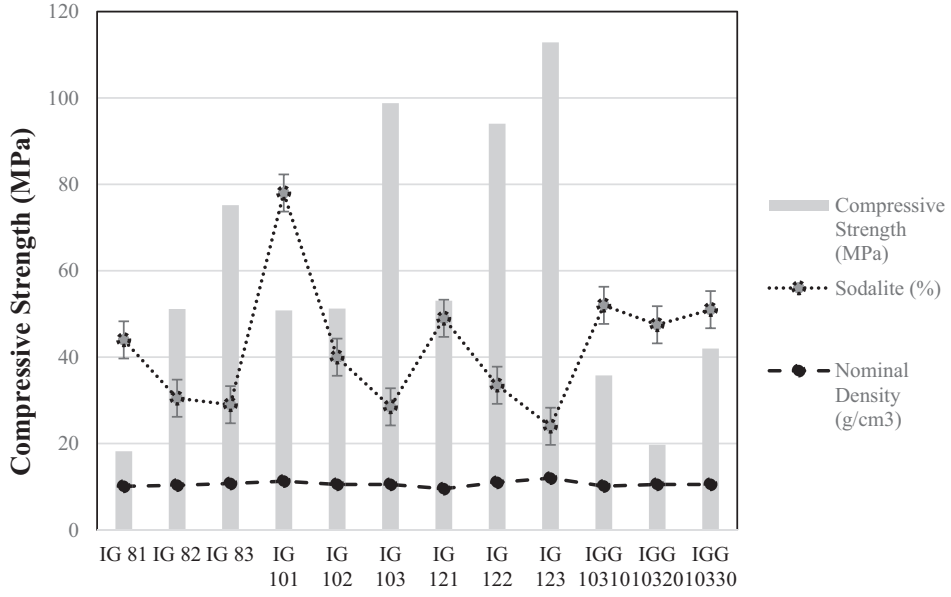

Fig. 9. Relation between compressive strength, zeolite (i.e., Sodalite) values, and nominal density.

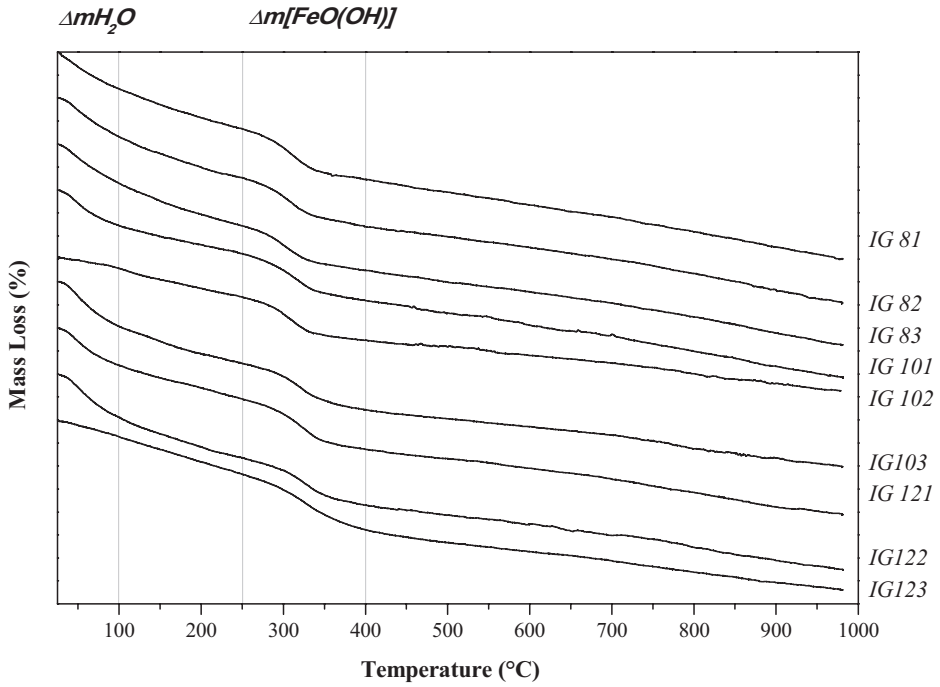

Fig. 10. TG analysis of IG specimens at 7 days of curing.

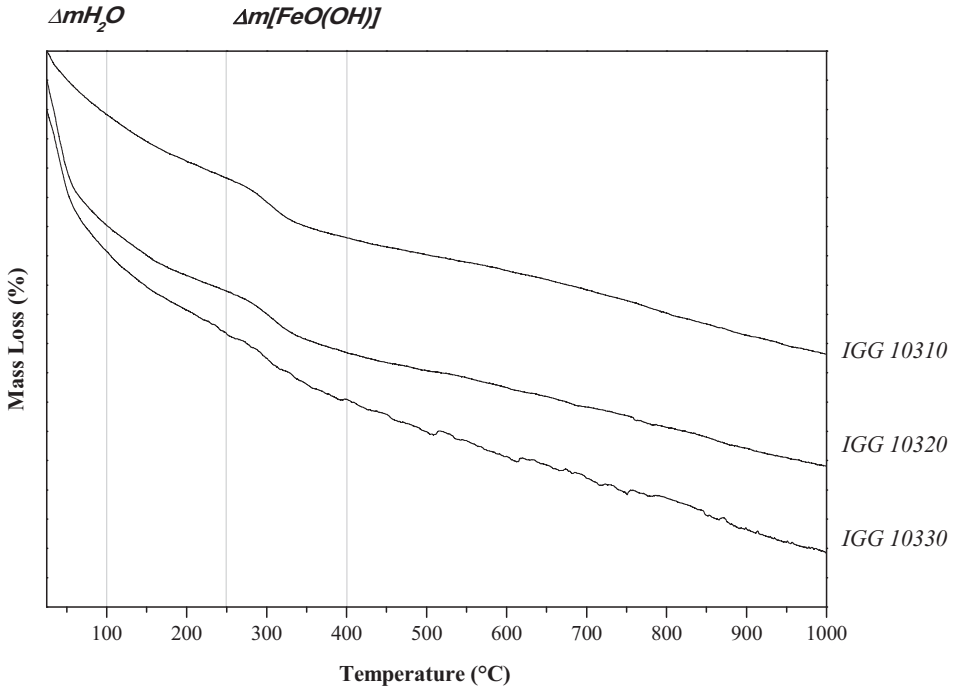

Fig. 11. TG analysis of IGG specimens at 7 days of curing.

indicates that GWR acted as a supplementary precursor material providing silica and aluminum to the geopolymeric synthesis.

The sodalite was also found in previous works on metakaolin-based geopolymer and was pointed as responsible for the low compressive strength [40]. Combined with mechanical results this fact reinforces the hypothesis of pack design been decisive on the mechanical properties development.

Confronting the results of compressive strength, sodalite content and nominal density (Fig. 9) is possible to observe the following trends: (a) the compressive strength decreases with the increase of sodalite crystallization; (b) the higher nominal density is related to the higher compressive strength; and (c) small increments in nominal density are related to high increases in compressive strength. As previously pointed, a well denser packing arrangement design, related to nominal density, is the primary factor to the mechanical property developments [13].

The TG results of all IG samples at 7 days of curing were clustered in Fig. 10. The thermal decomposition of IG geopolymers

Table 5
TG analysis of IOT, GWR, IG, and IGG specimens.

Mixture	Mass Loss (%)		
ID	0–100 °C	250–400 °C	0–1000 °C
GWR	0.20	1.47	4.18
IOT	0.36	1.55	6.02
IG 81	1.54	2.20	8.96
IG 82	1.69	2.12	8.94
IG 83	1.68	1.93	8.72
IG 101	1.53	2.03	8.18
IG 102	0.45	1.87	5.77
IG 103	1.93	2.00	8.06
IG 121	1.60	3.37	8.12
IG 122	1.86	2.05	8.51
IG 123	0.67	2.41	7.34
IGG 10310	2.13	2.05	10.38
IGG 10320	4.87	2.10	13.11
IGG 10330	4.74	2.23	15.06

displayed two mass losses at around 100 °C and 400 °C in the TG curves. These mass losses could be attributed to the evaporation of both free water and a part of the water chemically bonded to the geopolymer compounds, and dehydroxylation of goethite phase, respectively [45,46]. Likewise, the thermal decomposition of IGG geopolymer displayed two mass losses around 100 °C and 400 °C on the IGG's TG curves (Fig. 11). Compared to IG geopolymers, the IGG showed the peaks at the same temperature ranges with differences only on the values of mass loss.

Table 5 shows the mass losses of the IOT, GWR, IG geopolymers, and IGG geopolymers (these two lasts at 7 days of curing). The mass losses of the samples varied between 4.18% and 15.06%. The first mass loss increases as the substitution ratio increase, indicating the higher amounts of compounds related to the geopolymer synthesis. Furthermore, the increase on the mass loss in the temperature range of 100 °C observed in the IGG geopolymers may be related with the C—S—H precipitation yielded by the CaO available in the GWR [47]. The second peak decreases when the substitution ratio increases and this phenomenon could be attributed to the dilution factor since GWR partially replaces IOT.

The SEM micrographs of the IG 103 specimens are presented in Fig. 12. They show the presence of a small number of pores and inert particles (IP) embedded into geopolymer [Fig. 12(a)]. Fig. 12b shows microcracks, rough surfaces and the geopolymer gel covering the entire surface. Quartz and hematite act as inert material to geopolymer synthesis; thus, these inert particles are probably acting as fillers into the geopolymer composite. Furthermore, the high efficiency of the composite was probably a combined result of the reduced number of pores, the binder action of sodalite, geopolymeric compounds, the presence of inert particles working as filler, and the high packing density due to the particle size distribution.

The SEM micrographs of the specimens IGG 10310 and IGG 10320 are shown in Fig. 13. Fig. 13a shows inert particles and the presence of fiber particles (FP) related to the GWR. It is also observed a high number of pores compared to IG 103, a fact that could influence the mechanical performance. Fig. 13b shows a high magnification on the fiber particle, which exhibit the honeycomb-like aspect. This honeycomb-like structure can be attributed to C—S—H compounds as observed in previous studies [48]. Combining the SEM micrographs with TG/DTA analysis as well the brittle behavior tested in the flexural tests reinforces the thesis of C—S—H precipitation into the blended geopolymers synthesis.

The IGG 10320 shows a more homogeneous surface compared to the IG and IGG 10310 specimens, as well as the presence of fiber particles (FP) as shown on Fig. 13c. Magnified images on the fiber particle (Fig. 13d and e) show fiber surface under the synthesis process and a compound with gel aspect on the edges. It is observed a transformation process happening in the fiber-like particle, which can be attributed to GWR working as a supplementary precursor to the geopolymer synthesis forming particles with a honeycomb-like shape that could explain the brittle behavior of the IGG specimens.

Micrographs of the IGG 10330 specimens (Fig. 14) do not show fiber-like particles related to GWR. Additionally, they presented the most homogeneous aspect among all studied geopolymers (Fig. 14a). Using a high magnification (Fig. 14b) is observed some micropores, honeycomb structures, and the surface almost covered by geopolymers gel. The observed distinct particles in this work (Fig. 14c) are compatible with previously published images identified as being zeolite-type [49,50].

The current micrographs of the IGG samples indicate that GWR works as a supplementary precursor for the geopolymer synthesis instead of fiber reinforcement. In this sense, very different aspects were observed in comparison to previously reported SEM micrographs of fiber reinforced geopolymers [51,34]. As a result, the decrease in mechanical performance could be attributed to the honeycomb-like structures and/or the presence of pores observed in the SEM micrographs.

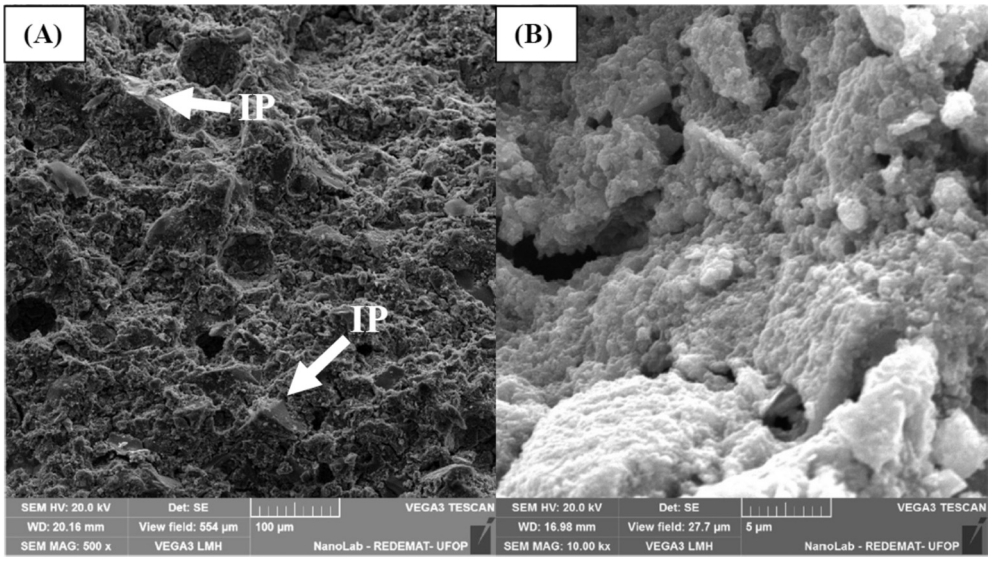

Fig. 12. SEM images of 7-days IG 103 with magnification of: (a) 500×; and (b) 10kx.

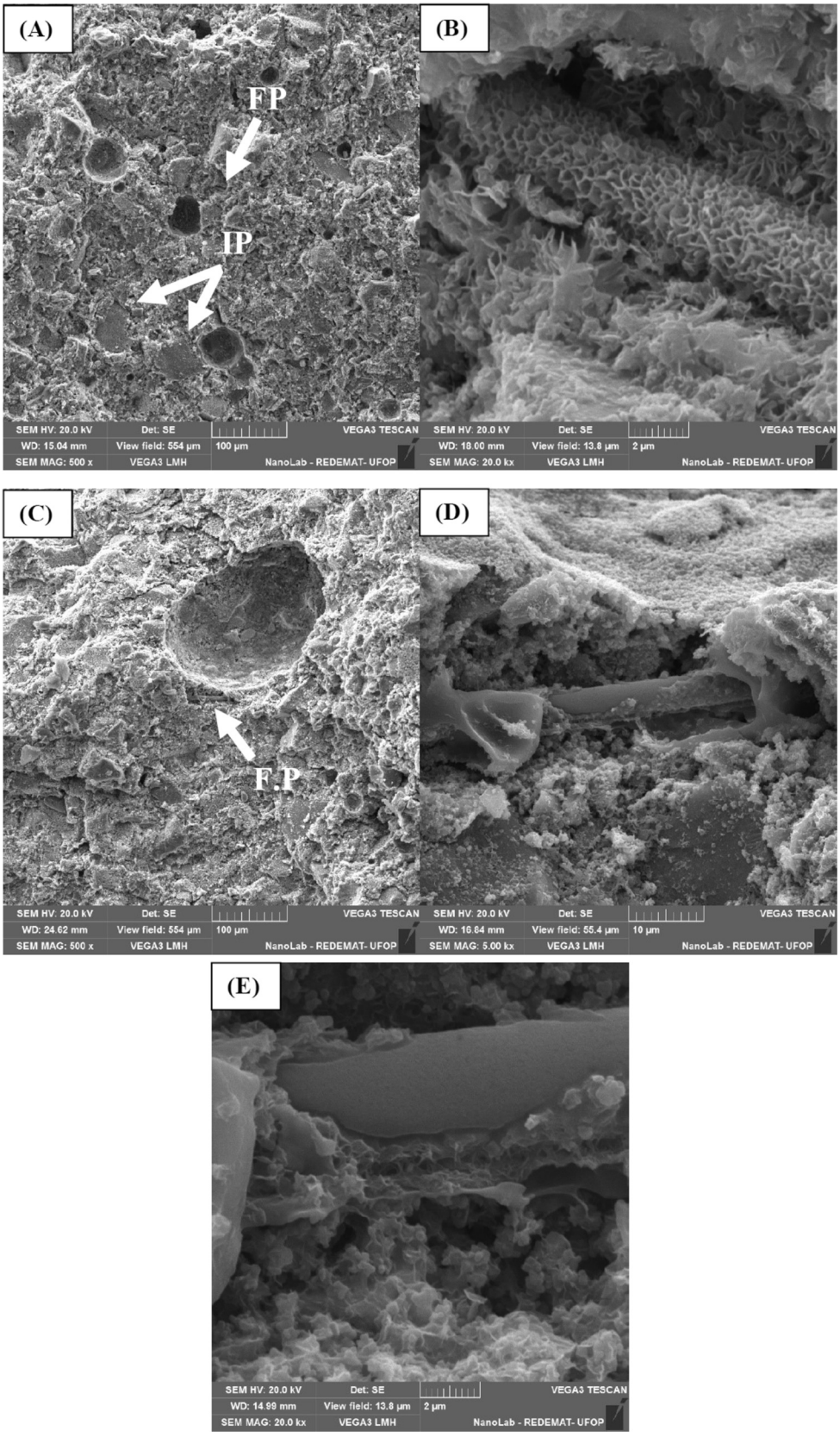

Fig. 13. SEM images of 7-days IGG: (a) 10310 magnification of 500x; (b) 10310 magnification of 20kx; (c) 10320 magnification of 500x; (d) 10320 magnification of 5kx; and (e) 10320 magnification of 20kx.

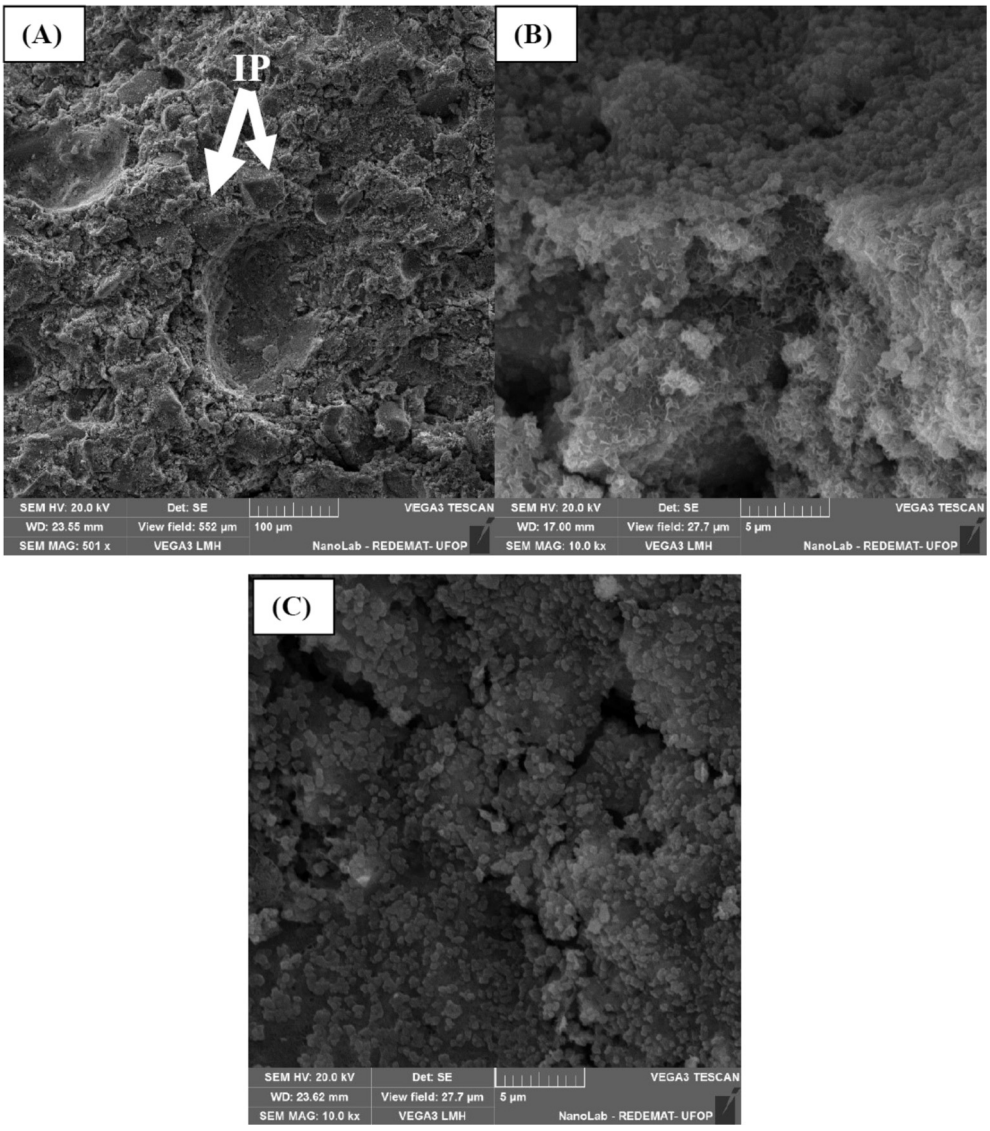

Fig. 14. SEM images of 7-days IGG 10330 with magnification of: (a) 500x; (b) 10 kx; and (c) 10 kx.

4. Conclusion

The geopolymers using IOT as primary source materials as well as the IOT-based geopolymer blended with GWR were studied in this paper. Experimental results showed high mechanical results and the potential to future application regarding the use of IOT and GWR in geopolymers production. The main findings are summarized as follows:

i. The use of IOT as precursor material yielded geopolymers with high compressive and flexural strength. The highest results obtained were 112.8 MPa and the 21.3 MPa for 7-days compressive strength and flexural strength, respectively. The partial replacement of IOT by GWR as supplementary precursor material led to a decrease on compressive strength and flexural strength for all substitution ratios. By the flexural strength of the blended geopolymer, we observed a brittle behavior related to the GWR presence. Through the mechanical results, the particle size distribution of the precursors and NaOH solution concentration played a great influence in mechanical performance.

ii. The XRD patterns showed a synthesis process of zeolite sodalite phase in all geopolymer specimens. Chamosite and partial chantalite were source phase to its synthesis; whereas, in the blended geopolymer both GWR's non-crystalline phase and IOT's crystalline phases contribute as precursor compounds to the geopolymeric reaction. The quartz, hematite and goethite phases in IOT works as inert phases to geopolymer composites.

iii. Thermal analysis of the IOT-based geopolymers showed increased mass losses related to the geopolymer compounds in all specimens. GWR blends yielded the highest mass losses in the range related to C—S—H and geopolymer compounds.

iv. SEM micrographs of the IOT-based geopolymers showed a composite with low porosity, structures related to geopolymeric reaction, inert particles embedded into the binder, and structures related to zeolite phases. In the SEM micrographs of the geopolymers blended with GWR, it was observed that the GWR particles work as supplementary precursor material and yield phases with gel aspect and honeycomb-like aspect related to C—S—H. Through the SEM micrographs of three different replacement ratios, it was possible to note the GWR transformation in two different stages.

This paper consists of an initial step for the application of IOT and GWR as precursor materials for geopolymer composites. Furthermore, the promising results that include composites with high mechanical performance already indicate good prospects for a new application of these residues, contributing to their proper destination, minimization of the use of landfills and tailing dams.

Declaration of Competing Interest

None.

Acknowledgements

We gratefully acknowledge the agencies CAPES for providing financial support; and the company VALE S.A. for the samples. We are also grateful for the infrastructure and collaboration of the Research Group in Solid Wastes – RECICLOS – CNPq.

The authors would like to acknowledge the Nanolab Electronic Microscopy Laboratory, at the REDEMAT – Escola de Minas; Laboratory of Thermal and Microscope Treatments of DEMET, UFOP, MG, Brazil, for providing the equipment and technical support for experiments involving Scanning Electron Microscope.

References

[1] B. Majidi, Geopolymer technology, from fundamentals to advanced applications: a review, Mater. Technol. 24 (2009) 79–87.
[2] P. Duxson, S. Mallicoat, G. Lukey, W. Kriven, J. van Deventer, The effect of alkali and Si/Al ratio on the development of mechanical properties of metakaolin-based geopolymers, Colloids Surf. A: Physicochem Eng. Aspects 292 (2007) 8–20.
[3] J. Davidovits, Geopolymers: inorganic polymeric new materials, J. Therm. Anal. Calorim. 37 (1991) 1633–1656.
[4] R. Iacobescu, D. Koumpouri, Y. Pontikes, R. Saban, G. Agelopoulos, Valorization of electric arc furnace steel slag as raw material for low energy belite cements, J. Hazard. Mater. 196 (2011) 287–294.
[5] M. Ali, M. Hossain, A review on emission analysis in cement industries, Renew. Sustain. Energy Rev. 15 (2011) 2252–2261.
[6] R. Kajaste, M. Hurme, Cement industry greenhouse gas emissions – management options and abatement cost, J. Cleaner Prod. 112 (2016) 4041–4052.
[7] José Maria Franco de Carvalho, Paula Anunciação Matias Campos, Keoma Defáveri, Guilherme Jorge Brigolini, Leonardo Gonçalves Pedroti, Ricardo André Fiorotti Peixoto, Low environmental impact cement produced entirely from industrial and mining waste, J. Mater. Civ. Eng. 31 (2) (2019) 04018391, https://doi.org/10.1061/(ASCE)MT.1943-5533.0002617.
[8] N. Ganesan, R. Abraham, S. Raj, Durability characteristics of steel fibre reinforced geopolymer concrete, Constr. Build. Mater. 93 (2015) 471–476.
[9] T. Bakharev, Resistance of geopolymer materials to acid attack, Cem. Concr. Res. 35 (2005) 658–670.
[10] T. Bakharev, Durability of geopolymer materials in sodium and magnesium sulfate solutions, Cem. Concr. Res. 35 (2005) 1233–1246.
[11] P. Duan, C. Yan, W. Zhou, D. Ren, Fresh properties, compressive strength and microstructure of fly ash geopolymer paste blended with iron ore tailing under thermal cycle, Constr. Build. Mater. 118 (2016) 76–88.
[12] N. Rajamane, M. Nataraja, N. Lakshamanan, J. Dattatreya, Rapid chloride permeability test on geopolymer and Portland cement, Indian Concr. J. 85 (2011) 21–26.
[13] A. Mehta, R. Siddique, An overview of geopolymers derived from industrial by-products, Constr. Build. Mater. 127 (2016) 183–198.
[14] FEAM, "Inventário estadual de barragens do estado de Minas Gerais," FEAM, Belo Horizonte, 2012.
[15] S. Alves, "A mineração está tentando fazer o seu dever de casa," VALE, 2009.
[16] W. Fontes, J. Mendes, D.S. Sidney, R. Peixoto, Mortars of laying and coating produced with iron ore tailings from tailing dams, Constr. Build. Mater. 112 (2016) 988–995.
[17] X. Huang, R. Ranade, W. Ni, V. Li, Development of green engineered cementitious composites using iron ore tailings as aggregates, Constr. Build. Mater. 44 (2013) 757–764.
[18] S. Zhao, J. Fan, W. Sun, Utilization of iron ore tailings as fine aggregate in ultra-high performance concrete, Constr. Build. Mater. 32 (2013) 540–548.
[19] Z. Yong-Chao, N. Wen, X. Li, L. De-Zhong, Y. Yong-Chao, Mechanochemical activation of iron ore tailings and preparation of high-strength construction materials, J. Univ. Sci. Technol. Beijing 32 (2010) 504–508.
[20] F. Silva, F. Araújo, M. Texeira, R. Gomes, F. Vonkruger, Study of the recovery and recycling of tailings from the concentration of iron ore for the production of ceramic, Ceram. Int. 40 (2014) 160850–216089.
[21] J. Galvao, H. Andrade, G. Brigolini, R. Peixoto, J. Mendes, Reuse of iron ore tailings from tailings dams as pigment for sustainable paints, J. Cleaner Prod. 200 (2018) 412–422.
[22] L. Weishi, L. Guoyuan, X. Ya, H. Qifei, The properties and formation mechanisms of eco-friendly brick building materials fabricated from low-silicon iron ore tailings, J. Cleaner Prod. 204 (2018) 685–692.
[23] K. Defáveri, J. Mendes, J. Carvalho, W. Fontes, R. Peixoto, G. Brigolini, Glass wool residue: a potential supplementary cementitious material, ACI Mater. J. (2019). In press.
[24] P. Duan, C. Yan, W. Zhou, D. Ren, Development of fly ash and iron ore tailing based porous geopolymer for removal of Cu(II) from wastewater, Ceram. Int. 42 (2016) 13507–13518.
[25] H. Rietveld, A profile refinement method for nuclear and magnetic structures, J. Appl. Crystallogr. 2 (1969) 65–71.
[26] NBR 13279, "Argamassa para assentamento e revestimento de paredes e tetos - Determinação da resistência à tração na flexão e à compressão," Associação Brasileira de Normas Técnicas, Rio de Janeiro, 2006.
[27] J. Davidovits, Geopolymer Chemistry & Applications, 4 ed., Institut Geopolymere, Saint-Quentin, France, 2008.
[28] P. De Silva, K. Sagoe-Crenstil, V. Sirivivatnanon, Kinetics of geopolymerization: role of Al2O3 and SiO2, Cem. Concr. Res. 37 (2007) 512–518.
[29] J. Provis, G. Lukey, S. van Deventer, Do geopolymers actually contain nanocrystalline zeolite? a reexamination of existing results, Chem. Mater. 17 (2005) 3075–3085.
[30] A. Shettima, M. Hussin, Y. Ahmad, J. Mirza, Evaluation of iron ore tailings as replacement for fine aggregate in concrete, Constr. Build. Mater. 120 (2016) 72–79.
[31] C. Li, H. Sun, J. Bai, L. Li, Innovative methodology for comprehensive utilization of iron ore tailings Part 1. The recovery of iron ore tailings using magnetic separation after magnetizing roasting, J. Hazard. Mater. 174 (2010) 71–77.
[32] F. Fan, Z. Liu, G. Xu, H. Peng, C. Cai, Mechanical and thermal properties of fly ash based geopolymers, Constr. Build. Mater. 160 (2018) 66–81.
[33] M. Al-Mashhadani, O. Canpolat, Y. Aygörmez, M. Uysal, S. Erdem, Mechanical and microstructural characterization of fiber reinforced fly ash based geopolymer composites, Constr. Build. Mater. 167 (2018) 505–513.
[34] A. Noushini, M. Hastings, A. Castel, F. Aslani, Mechanical and flexural performance of synthetic fibre reinforced geopolymer concrete, Constr. Build. Mater. 186 (2018) 454–475.
[35] J. He, Y. Jie, J. Zhang, Y. Yu, G. Zhang, Synthesis and characterization of red mud and rice husk ash-based geopolymer composites, Cem. Concr. Compos. 37 (2013) 108–118.
[36] A. Nazari, A. Bagheri, S. Riahi, Properties of geopolymer with seeded fly ash and rice husk bark ash, Mater. Sci. Eng., A 528 (2011) 7395–7401.
[37] P. Chindaprasirt, U. Rattanasak, P. Vondvoradit, S. Jenjirapanaya, Thermal treatment and utilization of Al-rich waste in high calcium fly ash geopolymeric materials, Int. J. Miner. Metall. Mater. 19 (2012) 872–878.
[38] T. Bakharev, Geopolymeric materials prepared using Class F fly ash and elevated temperature curing, Cem. Concr. Res. 35 (2005) 1224–1232.
[39] S. Ahmari, L. Zhang, Production of eco-friendly bricks from copper mine tailings through geopolymerization, Constr. Build. Mater. 29 (2012) 323–331.
[40] I. Ozer, S. Soyer-Uzun, Relations between the structural characteristics and compressive strength in metakaolin based geopolymers with different molar Si/Al ratios, Ceram. Int. 41 (2015) 10192–10198.
[41] J. Buhl, T. Gesing, I. Kerkamm, C. Gurris, Synthesis and crystal structure of cyanate sodalite [Na8 (OCN)2/[Al6Si6O24], Microporous Mesoporous Mater. 65 (2003) 145–153.
[42] N. Lee, R. Khalid, H. Lee, Synthesis of mesoporous geopolymers containing zeolite phases by a hydrothermal treatment, Microporous Mesoporous Mater. 15 (2016) 22–30.
[43] B. Fultz, J. Howe, Transmission electron microscopy and diffractometry of materials, Springer-Verlag, Berlin, 2002.
[44] C. Rios, C. Williams, O. Alarcón, Nucleation and growth process of sodalite and cancrinite from kaolinite-rich clay under low-temperature hydrothermal conditions, Mater. Res. 16 (2013) 424–438.
[45] H. Liu, T. Chen, X. Zou, C. Qing, R. Frost, Thermal treatment of natural goethite: thermal transformation and physical properties, Thermochim. Acta 568 (2013) 115–121.
[46] T. Rocha, D. Dias, F. França, R. Guerra, L. Marques, Metakaolin-based geopolymer mortars with different alkaline activators (Na+ and K+), Constr. Build. Mater. 178 (2018) 453–461.
[47] R. Kaminskas, V. Cesnaukas, R. Kubiliute, Influence of different artificial additives on Portland cement hydration and hardening, Constr. Build. Mater. 95 (2015) 537–544.
[48] R. Drochytka, E. Helanova, Development of microstructure of the fly ash aerated concrete in time, Procedia Eng. 108 (2015) 624–631.
[49] C. Ríos, C. Williams, M. Fullen, Nucleation and growth history of zeolite LTA synthesized from kaolinite by two different methods, Appl. Clay Sci. 42 (2009) 446–454.
[50] Z. Zhang, H. Wang, J. Provis, F. Bullen, A. Reid, Y. Zhu, Quantitative kinetic and structural analysis of geopolymers. Part 1. The activation of metakaolin with sodium hydroxide, Thermochim. Acta 539 (2012) 23–33.
[51] W. Punurai, W. Kroehong, A. Saptamongkol, P. Chindaprasirt, Mechanical properties, microstructure and drying shrinkage of hybrid fly ash-basalt fiber geopolymer paste, Constr. Build. Mater. 186 (2018) 62–70.